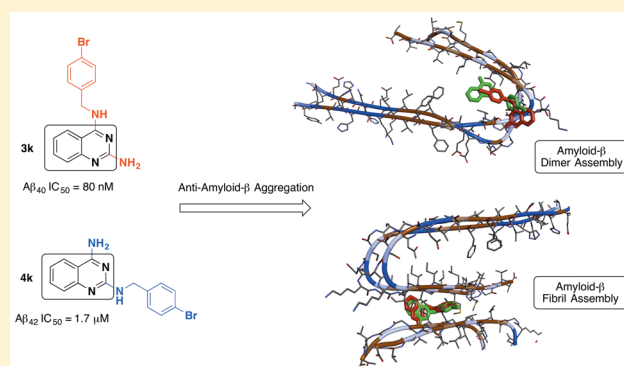


Structure–Activity Relationship Studies of Isomeric 2,4-Diaminoquinazolines on  $\beta$ -Amyloid Aggregation KineticsTarek Mohamed,<sup>†,‡</sup> Arash Shakeri,<sup>†</sup> Gary Tin,<sup>†</sup> and Praveen P. N. Rao<sup>\*,†</sup><sup>†</sup>School of Pharmacy, Health Sciences Campus, and <sup>‡</sup>Department of Chemistry, University of Waterloo, 200 University Avenue West, Waterloo, Ontario N2L 3G1, Canada

## Supporting Information

**ABSTRACT:** A library of isomeric 2,4-diaminoquinazoline (DAQ) derivatives were synthesized and evaluated for antiaggregation potential toward A $\beta$ 40/42. Structure–activity relationship data identified compound **3k** (*N*<sup>1</sup>-(4-bromobenzyl)quinazoline-2,4-diamine) with a 4-bromobenzyl substituent as the most potent inhibitor (A $\beta$ 40 IC<sub>50</sub> = 80 nM) and was almost 18-fold more potent compared to the reference agent curcumin (A $\beta$ 40 IC<sub>50</sub> = 1.5  $\mu$ M). The corresponding *N*<sup>2</sup>-isomer **4k** (*N*<sup>2</sup>-(4-bromobenzyl)quinazoline-2,4-diamine) was also able to prevent A $\beta$  aggregation (A $\beta$ 40 IC<sub>50</sub> = 1.7  $\mu$ M). However, compound **4k** exhibited superior inhibition of A $\beta$ 42 aggregation (A $\beta$ 42 IC<sub>50</sub> = 1.7  $\mu$ M) compared to compound **3k** (A $\beta$ 42 IC<sub>50</sub> = 14.8  $\mu$ M) and was  $\sim$ 1.8-fold more potent compared to curcumin (A $\beta$ 42 IC<sub>50</sub> = 3.1  $\mu$ M). These results were supported by A $\beta$  aggregation kinetics investigations and transmission electron microscopy studies, which demonstrate the suitability of DAQ ring system to develop anti-amyloid agents as pharmacological tools to study A $\beta$  aggregation.

**KEYWORDS:** Quinazolines, amyloid, A $\beta$  aggregation, Alzheimer's disease



One of the most influential hallmarks of Alzheimer's pathology is the collapse of cellular amyloid management, leading to the progressive accumulation of neurotoxic A $\beta$ -deposits.<sup>1–4</sup> While the mechanisms intertwining the amyloid pathway are vast and complex, a number of strategies to combat its neuronal insults have been proposed, researched, and evaluated in various preclinical and clinical settings.<sup>5–7</sup> An essential tool utilized by researchers to further understand the aggregation mechanisms of amyloidogenic peptides, such as A $\beta$ , is to develop and evaluate aggregation modulators and inhibitors.<sup>8,9</sup> Not only is this beneficial in understanding the kinetics of amyloid aggregation but it may reveal potential therapeutic candidates.

When it comes to developing drug candidates, nature plays an important role in highlighting ideas for potential core templates and scaffolds. Honing in on the case of A $\beta$  with respect to aggregation modulators and inhibitors, compounds such as curcumin, a component of the spice turmeric, and resveratrol, a phytoalexin found in grapes and berries (Figure 1), are considered as model compounds in this context.<sup>10–13</sup> The synthetic compound, orange G is a commonly used stain/dye and, like curcumin and resveratrol, is used as a pharmacological tool in drug discovery due to its excellent activity against amyloid aggregation.<sup>14,15</sup>

From a chemical standpoint, these small molecules share structural features including aromaticity, conjugation, and planarity resulting in their ability to intercalate and disrupt

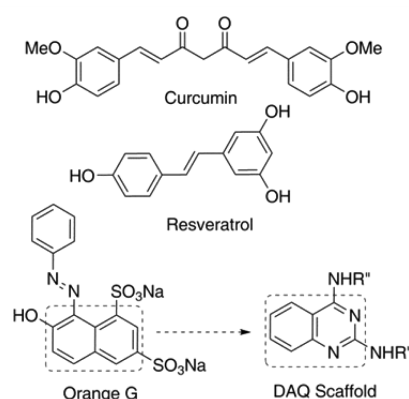


**Figure 1.** Structures of naturally occurring and synthetic amyloid aggregation inhibitors and the DAQ scaffold.

the backbone hydrogen bonding interactions in the beta-sheet assembly thereby providing a framework to design small molecules as pharmacological tools to study A $\beta$  aggregation and inhibition.<sup>16,17</sup> As part of our research program aimed at discovering and developing novel small-molecules as potential pharmacological tools to study Alzheimer's disease (AD) and

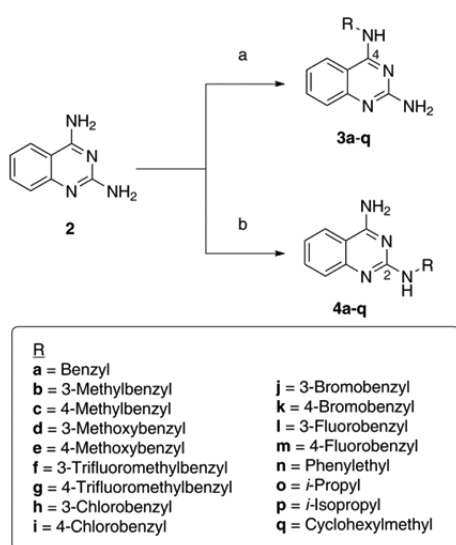
**Received:** January 26, 2016

**Accepted:** March 1, 2016

**Published:** March 1, 2016

design novel anti-AD agents, we embarked on the development of isomeric 2,4-diamino-quinazolines (DAQ) library as a novel class of compounds that exhibit anti- $A\beta$  aggregation properties. The planar, bicyclic quinazoline ring template can be considered as a bioisostere of the naphthalene ring present in orange G (Figure 1). A library of 34 isomeric DAQs were synthesized and their anti- $A\beta$  aggregation activity was evaluated by monitoring the  $A\beta_{40}$  and  $A\beta_{42}$  aggregation kinetics using ThT-fluorescence and by transmission electron microscopy (TEM) measurements. Computational experiments were used to propose their binding interactions with  $A\beta$ -aggregates. These studies show that the anti- $A\beta$  activity was sensitive to isomeric placement of substituents either at the 2 or 4-position of the quinazoline amine template and that they represent a novel class of compounds that can be useful to design small molecules with anti-amyloid aggregation properties.

The DAQ template (**2**, Scheme 1) was synthesized starting from 2-fluoro (**1a**) or 2-aminobenzonitrile (**1b**) by heating with

Scheme 1<sup>a</sup>

<sup>a</sup>Reagents and conditions: (a) Alkyl- or aromatic halides, NaH, DMSO, 0 °C to r.t. 14 h. (b) Alkyl- or aromatic halides, potassium carbonate, DMA, r.t. to 85 °C, 5 h.

excess guanidine carbonate in dimethylacetamide (DMA) under pressure (Scheme S1, Supporting Information).<sup>18,19</sup> The reaction with 2-fluorobenzonitrile provided superior yield (~70%) of **2** compared to 2-aminobenzonitrile (~40%). The most challenging aspect of this synthesis was developing selective alkylation methods to prepare either  $N^2$ - or  $N^4$ -substituted quinazoline amines. After investigating a variety of base, solvent, time, and temperature combinations (Table S1, Supporting Information), two selective conditions were identified. Using NaH and DMSO provided the  $N^4$ -isomer exclusively, whereas combination of potassium carbonate and DMA favored the  $N^2$ -isomer exclusively (Scheme 1). Their chemical structures were confirmed by <sup>1</sup>H, <sup>13</sup>C NMR, and 2D COSY NMR studies. These studies show that the  $N^4$ -NHs are more acidic ( $\delta$  7.74 ppm) compared to the  $N^2$ -NH protons ( $\delta$  6.53 ppm).

The conditions used for selective alkylation provided low yield (14–31%). The TLC examinations showed that the reactions did not go to completion. Attempts to increase the

yield by increasing the base equivalence along with that of the R-groups resulted in mixed isomers and/or double substitutions as confirmed by NMR studies. Based on these observations, selective alkylation at either  $N^2$  or  $N^4$ -position was achieved using  $K_2CO_3$ /DMA and NaH/DMSO, respectively, using various substrates (Scheme 1, R = benzyl, substituted benzyl, phenethyl, *n*-Pr, *i*-Pr, or cyclohexylmethyl). Attempts at synthesizing the  $N^2$ - or  $N^4$ -methylpyridyl based DAQ compounds using the same conditions were not successful. The assessment of these isomeric DAQ derivatives against the self-induced aggregation mechanisms of both  $A\beta_{40}$  and  $A\beta_{42}$  revealed a combination of structure–activity relationships (SARs). As shown in Table 1, the aggregation  $IC_{50}$  values are listed for each derivative and were compared with standard controls (orange G, curcumin, resveratrol) and the DAQ template itself. Examining the SAR data obtained based on a thioflavin T (ThT) based fluorescence spectroscopy method (Table 1) demonstrates the overall ability of these  $N^2$ - and  $N^4$ -substituted DAQ derivatives to inhibit the aggregation of amyloid peptides. In contrast, the DAQ template alone (Table 1) was promoting the aggregation process. Generally,  $N^4$ -substituted DAQ derivatives (**3a–q**) were more effective at inhibiting  $A\beta_{40}$  compared to their  $N^2$ -substituted isomers (**4a–q**). Interestingly, this observation is completely reversed with respect to  $A\beta_{42}$ . The addition of a benzyl substituent either at  $N^4$ - or  $N^2$ -position in compounds **3a** and **4a** provided  $A\beta_{40}$  aggregation inhibition (Table 1). However, the  $N^4$ -regioisomer **3a** did not exhibit any inhibition of  $A\beta_{42}$  unlike the  $N^2$ -regioisomer **4a**. The  $N^2$ -placement in **4a** was more effective against  $A\beta_{42}$  ( $IC_{50}$  = 8.4  $\mu$ M). Replacing the benzyl substituent with a more lipophilic 3- or 4-methylbenzyl substituent in **3b**, **3c** and **4b**, **4c** modified the biological profiles significantly. When compared to **3a**, the  $N^4$ -placement of a methylbenzyl substituent, regardless of *meta*- or *para*-positioning, slightly improved activity against  $A\beta_{40}$  (no more than ~1.3-fold improvement) with no change toward  $A\beta_{42}$ . This was not the case with the  $N^2$ -isomers, where the methyl-substituted benzyl group resulted in loss of activity against both  $A\beta_{40}$  and  $A\beta_{42}$  (**4b**,  $A\beta_{40/42}$   $IC_{50}$  > 25  $\mu$ M) or a much weaker profile (**4c**,  $A\beta_{40}$   $IC_{50}$  = 13.1  $\mu$ M,  $A\beta_{42}$   $IC_{50}$  = 22.5  $\mu$ M) compared to **4a** (Table 1). The addition of an electron-donating methoxybenzyl group, in **3d**, **3e** and **4d**, **4e**, yielded mixed outcomes. The  $N^4$ -placement of a 3-methoxybenzyl group (**3d**,  $A\beta_{40}$   $IC_{50}$  = 20.6  $\mu$ M,  $A\beta_{42}$   $IC_{50}$  = inactive at 25  $\mu$ M) was detrimental to antiaggregation activity compared to the benzyl derivative **3a**, while the 4-methoxybenzyl substituent (**3e**,  $A\beta_{40}$   $IC_{50}$  = 1.1  $\mu$ M,  $A\beta_{42}$   $IC_{50}$  > 25  $\mu$ M) enhanced the activity against  $A\beta_{40}$  by ~4–4.5-fold (compared to **3a** and **3c**). However,  $N^2$ -placement of the 3-methoxy-substituted benzyl group (**4d**,  $A\beta_{40/42}$   $IC_{50}$  > 25  $\mu$ M) did not offer any benefits compared to **4a** and was ineffective in providing antiaggregation activity. The 4-methoxy compound (**4e**,  $A\beta_{40}$   $IC_{50}$  = 6.8  $\mu$ M,  $A\beta_{42}$   $IC_{50}$  > 25  $\mu$ M) was ~6-fold less potent compared to its  $N^4$ -isomer (**3e**) toward  $A\beta_{40}$ .

The effect of electron-withdrawing trifluoromethylbenzyl substituent was investigated in compounds **3f**, **3g** and **4f**, **4g**. Interestingly, its presence at  $N^4$ -position in compound **3f** (3-CF<sub>3</sub>-benzyl) provided similar inhibition profile compared to **3b** (3-Me) with  $IC_{50}$  values around 3.6  $\mu$ M for  $A\beta_{40}$  and over 20  $\mu$ M for  $A\beta_{42}$ . This was not the case with **3g** (4-CF<sub>3</sub>), which was ~2-fold more potent toward  $A\beta_{40}$  compared to its methylbenzyl bioisostere (**3c**). However, this modification did not provide better inhibition of  $A\beta_{42}$ . With  $N^2$ -placement,

Table 1. Inhibition Data for DAQ Isomeric Derivatives 3a–q and 4a–q against Self-Induced A $\beta$ 40 and A $\beta$ 42 Aggregation

3a-q vs. 4a-q

N <sup>4</sup> -isomer	IC <sub>50</sub> (μM) <sup>a,b</sup>		R-group	IC <sub>50</sub> (μM) <sup>a,b</sup>		N <sup>2</sup> -isomer
	A $\beta$ 40	A $\beta$ 42		A $\beta$ 40	A $\beta$ 42	
3a	4.8	>25	benzyl	2.2	8.4	4a
3b	3.6	>25	3-Me-benzyl	>25	>25	4b
3c	3.9	>25	4-Me-benzyl	13.1	22.5	4c
3d	20.6	n.a	3-OMe-benzyl	>25	>25	4d
3e	1.1	>25	4-OMe-benzyl	6.8	>25	4e
3f	3.5	21.0	3-CF <sub>3</sub> -benzyl	12.5	13.8	4f
3g	1.9	>25	4-CF <sub>3</sub> -benzyl	2.3	5.3	4g
3h	1.9	>25	3-Cl-benzyl	5.9	13.4	4h
3i	0.62	>25	4-Cl-benzyl	0.93	8.1	4i
3j	0.58	22.3	3-Br-benzyl	1.5	2.7	4j
3k	0.08	14.8	4-Br-benzyl	1.7	1.7	4k
3l	2.8	>25	3-F-benzyl	11.3	14.7	4l
3m	3.1	>25	4-F-benzyl	>25	>25	4m
3n	7.8	>25	phenethyl	14.9	>25	4n
3o	14.9	n.a	<i>n</i> -Pr	>25	>25	4o
3p	10.2	n.a	<i>i</i> -Pr	>25	>25	4p
3q	13.6	>25	cyclohexylmethyl	>25	>25	4q
DAQ	P.A	P.A		1.5	3.1	curcumin
orange G	3.0	8.7		2.6	4.1	resveratrol

<sup>a</sup>IC<sub>50</sub> values are calculated based on the ThT-based fluorescence spectroscopy assay (excitation = 440 nm, emission = 490 nm). <sup>b</sup>Values are mean values of triplicate readings for three independent experiments. n.a = not active. P.A = promotes aggregation.

however, the modification from (3/4-Me) to (3/4-CF<sub>3</sub>) was positive across the board. While **4b** was ineffective against both A $\beta$ 40/42 (IC<sub>50</sub> > 25 μM), **4f** (3-CF<sub>3</sub>) was active toward both species (IC<sub>50</sub> ≈ 12–13 μM). Derivative **4g**, however, was more potent compared to **4c** (4-Me), equipotent to **4a** (A $\beta$ 40), and ~1.6-fold more potent toward A $\beta$ 42 compared to **4a**. It exhibited equipotent/comparable activity to the reference compound resveratrol (Table 1). In the next set of compounds, the effect of benzyl halides at N<sup>2</sup> and N<sup>4</sup>-position was explored. Generally, the presence of benzyl halides increased overall inhibition potency (with the exception of fluorobenzyl). Starting with the N<sup>4</sup>-placement of 3-chloro (**3h**) or 4-chlorobenzyl (**3i**) substituents, both were more potent toward A $\beta$ 40 compared to **3a** (~2.5-fold and ~8-fold, respectively). In this regard **3i** exhibited potent inhibition of A $\beta$ 40 with an IC<sub>50</sub> = 620 nM and was approximately 2.4-fold more potent compared to the reference agent curcumin (A $\beta$  IC<sub>50</sub> = 1.5 μM). However, both **3i** and **3h** were ineffective against A $\beta$ 42 (IC<sub>50</sub> > 25 μM). Interestingly, the N<sup>2</sup>-placement of these chlorobenzyl groups (**4h/4i**) exhibit inhibition of both A $\beta$ 40 and A $\beta$ 42 aggregation. They were not as potent as **3i** and **3h** against A $\beta$ 40 (Table 1). The bromine-based bioisosteres (**3j**, **3k** and **4j**, **4k**) were all more potent against both A $\beta$ 40/42 compared to their chlorine-based counterparts with one exception (**4k** on A $\beta$ 40, Table 1). Derivative **3k** (4-bromobenzyl) was identified as the most potent A $\beta$ 40 aggregation inhibitor (IC<sub>50</sub> ≈ 80 nM). It was ~7.5-fold more potent compared to its 3-bromobenzyl isomer (**3j**, A $\beta$ 40 IC<sub>50</sub> = 580 nM, A $\beta$ 42 IC<sub>50</sub> = 22.3 μM) and ~21-fold more potent compared to its N<sup>2</sup>-isomer (**4k**, A $\beta$ 40 and A $\beta$ 42 IC<sub>50</sub> = 1.7 μM). Both **3k** and **3j** were much more potent inhibitors compared to reference agents orange G, curcumin,

and resveratrol. Furthermore, placing the 3-bromobenzyl substituent at N<sup>2</sup>-position, significantly enhances the A $\beta$ 42 aggregation inhibition in compound **4j** (A $\beta$ 40 IC<sub>50</sub> = 2.7 μM) with almost 8-fold gain in activity compared to the corresponding N<sup>4</sup>-isomer **3j** (A $\beta$ 42 IC<sub>50</sub> = 22.3 μM, Table 1). In contrast, the presence of an electronegative fluorobenzyl substituent at either N<sup>2</sup>- or N<sup>4</sup>-position was detrimental suggesting that smaller size of a fluorine atom compared to either a bromine or chlorine atom was not favorable. The N<sup>4</sup>-derivatives **3l** and **3m** were ineffective against A $\beta$ 42. Although they lost considerable activity toward A $\beta$ 40, they did maintain moderate levels of inhibition (IC<sub>50</sub> ≈ 3 μM) comparable to the methyl- (**3b**, **3c**) and trifluoromethyl-based derivatives (**3f**, **3g**). The extent of activity loss was greater with N<sup>2</sup>-placements, where derivative **4l** exhibited weak activity toward both A $\beta$ 40/42 (IC<sub>50</sub> ≈ 11–15 μM) and **4m** was ineffective against both A $\beta$ 40/42 (Table 1). In other SAR modifications, the addition of a methylene group (phenethyl vs benzyl) in compounds **3n** and **4n**, did not improve the A $\beta$  inhibitory activity compared to **3a** and **4a** (Table 1). Compound **3n** was ~1.6-fold less potent toward A $\beta$ 40 compared to **3a** and not very effective toward A $\beta$ 42 either. This modification also caused a loss of A $\beta$ 42 inhibitory activity for **4n** along with a ~ 6.7-fold decrease in potency toward A $\beta$ 40. Similarly, the addition of alkyl substituents (*n*-Pr and *i*-Pr) either at N<sup>2</sup>- or N<sup>4</sup>-position, as seen in compounds **3o**, **3p** and **4o**, **4p** resulted in either weak or no inhibition of aggregation (Table 1). Furthermore, the addition of a cyclic nonaromatic substituent such as a cyclohexylmethyl group (compound **3q** and **4q**) was detrimental to antiaggregation activity clearly displaying the

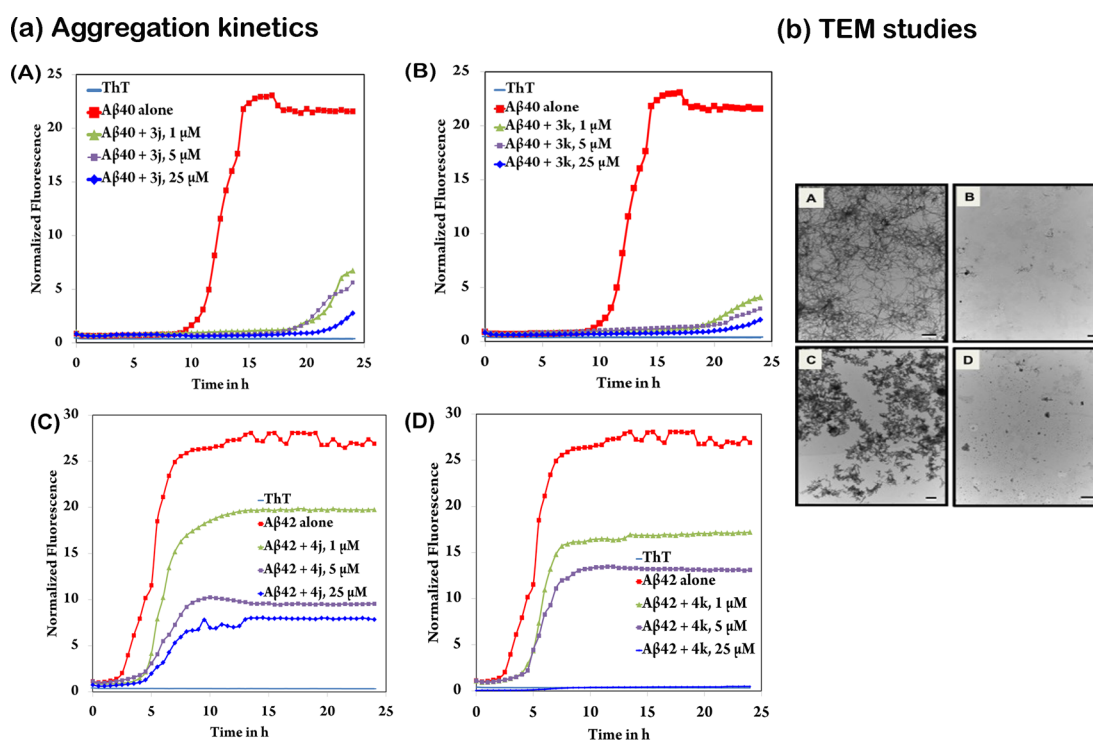


**Figure 2.** (a) Amyloid aggregation kinetics study. Panels A and B: 5  $\mu\text{M}$   $A\beta 40$  with varying concentrations (1, 5, or 25  $\mu\text{M}$ ) of DAQ derivatives **3j** and **3k**, respectively. Panels C and D: 5  $\mu\text{M}$   $A\beta 42$  with varying concentrations (1, 5, or 25  $\mu\text{M}$ ) of DAQ derivatives **4j** and **4k**, respectively. Aggregation kinetics were monitored by ThT-fluorescence spectroscopy (excitation = 440 nm, emission = 490 nm) for 24 h at 37  $^{\circ}\text{C}$  in phosphate buffer at pH 7.4. Results are based on three independent experiments in triplicate measurements. (b) Amyloid morphology analysis using transmission electron microscopy (TEM) after 24 h incubation at 37  $^{\circ}\text{C}$  in phosphate buffer at pH 7.4. Panel A, 25  $\mu\text{M}$   $A\beta 40$  control; Panel B, 25  $\mu\text{M}$   $A\beta 40$  with 25  $\mu\text{M}$  of DAQ derivative **3k**; Panel C, 25  $\mu\text{M}$   $A\beta 42$  control; Panel D, 25  $\mu\text{M}$   $A\beta 42$  with 25  $\mu\text{M}$  of DAQ derivative **4k**. Scale: black/white bars represent 500 nm.

importance of having planar aromatic substituents to exhibit antiaggregation properties.

In summary, based on this SAR study, we identified a total of nine DAQ based compounds (**3e**, **3g–k**, and **4i–k**) that exhibited superior or equipotent anti- $A\beta$  aggregation activity profile compared to reference agents orange G, curcumin, and resveratrol (Table 1). Compounds **4j** and **4k** met or surpassed the  $A\beta 42$  activity seen with curcumin (the most potent among the reference agents used), while a total of 9 derivatives (**3e**, **3g–k** and **4i–k**) closely met or surpassed the  $A\beta 40$  activity shown by the same reference agents. Derivative **3k**,  $N^4$ -(4-bromobenzyl)quinazoline-2,4-diamine, was identified as the most potent  $A\beta 40$  aggregation inhibitor ( $\text{IC}_{50} \approx 80$  nM), while its  $N^2$ -isomer,  $N^2$ -(4-bromobenzyl)quinazoline-2,4-diamine (**4k**), was identified as the most potent and dual  $A\beta 40/42$  aggregation inhibitor ( $\text{IC}_{50} \approx 1.7$   $\mu\text{M}$ ).

To better understand the modes of inhibition exerted by **3k** and **4k** (and their regioisomers **3j** and **4j**), we investigated the full aggregation kinetic plots (Figure 2a, panels A–D, and Figure S1, Supporting Information) derived from the ThT based aggregation assay used to determine the  $\text{IC}_{50}$  values listed in Table 1. The assessment of the kinetic plots provided greater insight into the potential mode of action for this class of compounds. The aggregation kinetic plots for compounds **3j** and **3k** (Figure 2a, panels A and B) show that both of these derivatives achieve their superior inhibitory activity by stabilizing the monomeric  $A\beta 40$  structures. The half time ( $t_{50}$ ) that defines the time at which the fluorescence intensity reaches the midpoint between pre- and postaggregation baseline growth phase in the absence of test compounds was

approximately 12.5 h for  $A\beta 40$  control curve. In this regard, both compounds **3j** and **3k** were able to prevent the nucleation-dependent aggregation process significantly, with a relatively weak growth phase seen toward the end of the 24 h aggregation period. Significantly, both of these compounds were exhibiting potent anti-amyloid aggregation properties at all the tested concentrations (1, 5, and 25  $\mu\text{M}$ , Figure 2a, panels A and B). The aggregation kinetics plot of the corresponding  $N^2$ -isomers **4j** and **4k** (Figure S1, panels A and B, Supporting Information) displayed concentration-dependent inhibition via improving monomer stability and reducing the rate of aggregation; however, the antiaggregation effect was not as drastic as compounds **3j** and **3k**. Compound **4j** at 25  $\mu\text{M}$  was able to delay the aggregation compared to  $A\beta$  control curve ( $t_{50} \approx 17$  h vs 12.5 h for  $A\beta$  control with no test compound), whereas **4k** at 25  $\mu\text{M}$  was able to exhibit complete inhibition of  $A\beta 40$  aggregation. These studies demonstrate that at 25  $\mu\text{M}$ ,  $N^4$ -isomers, compounds **3j**, **3k**, and the  $N^2$ -isomer **4k** were capable of preventing the formation of  $A\beta$  aggregates including dimers, trimers, oligomers, protofibrils, and fibrils.

With respect to  $A\beta 42$ , the dominance of the  $N^2$ -isomers (**4j** and **4k**, Figure 2a, panels C and D) became evident when compared to their  $N^4$ -counterparts (**3j** and **3k**, Figure S1, panels C and D, Supporting Information). The half time  $t_{50}$  was approximately 2 h for  $A\beta 42$  in the absence of test compounds. In this regard, compounds **3j** and **3k** were able to delay the lag phase to a great extent ( $t_{50}$  values of approximately 2.6 and 3.5 h, respectively, at 25  $\mu\text{M}$  compared to  $A\beta 42$  control). In contrast, the  $N^4$ -isomers **4j** and **4k** exhibited better inhibition profile with compound **4j** showing a significant delay in

aggregation ( $t_{50} \approx 6$  h), whereas **4k** was able to show complete inhibition at 25  $\mu\text{M}$  (Figure 2a, panels C and D). While all the kinetic plots for A $\beta$ 42 demonstrated concentration-dependent inhibition, none of these derivatives were capable of completely halting the saturation phase except for the  $N^2$ -isomer **4k** at the highest concentration tested.

To further validate these observations, A $\beta$ 40/42 morphology was assessed using transmission electron microscopy (TEM, Figure 2b, Figure S2 and S3, Supporting Information) in the presence and absence of most potent DAQ derivatives (**3j**, **3k**, **4j**, and **4k**, Figure 2b and Figure S2, Supporting Information). As observed with TEM, both A $\beta$ 40/42 control samples (25  $\mu\text{M}$ ) displayed high levels of dense and full aggregate species. Coincubation experiments with DAQ derivatives (**3j**, **3k**, **4j** and **4k**), at 25  $\mu\text{M}$ , were able to drastically hinder the aggregation process with the  $N^4$ -isomer **3k** (Figure 2b, panel B) and  $N^2$ -isomer **4k** (Figure 2b, panel D) exhibiting almost complete inhibition of aggregation. These results correlate with the ThT aggregation kinetics data (Figure 2a and Figure S1, Supporting Information).

In order to gain some insights into the mechanism of anti-A $\beta$  aggregation properties of DAQ derivatives (**3j**, **3k**, **4j**, and **4k**), we investigated their binding interactions in both the A $\beta$  dimer and A $\beta$  fibril model (Figures S4 and S5, Supporting Information). In the dimer model (Figure S4, panels A and B, Supporting Information), featuring the A $\beta_{9-40}$  fragment,<sup>20</sup> each of the docked DAQ derivatives interacted with the dimeric structure in a unique fashion, although these interactions were generally localized in the dimer-turn region (Asp23-Gly29). This might explain the trends seen in the kinetic plots, where monomer stability and substantial delays in the aggregation process were observed. The DAQ ring scaffold of **3j** was oriented between Phe20 (perpendicular to the phenyl ring) and Val24 (distance  $\sim 5-7$  Å), where the 3-bromophenyl ring was aligned, in a parallel fashion, toward Ser26 and Asn27 (distance  $\approx 5$  Å). The bromine atom was oriented toward Ile32-Leu34 pocket at the C-terminal end (Figure S4, panel A). The C2-amine was positioned across from Val24-Gly25 on the adjacent monomer (distance  $\approx 5$  Å). However, the corresponding  $N^2$ -isomer **4j** had its DAQ ring scaffold between Asp23 and Lys28 (distance  $\approx 5$  Å), where the C4-amine was undergoing hydrogen-bonding interaction with Asp23 (distance  $< 3$  Å). The 3-bromophenyl ring was oriented toward Asp23 and Val24 (distance  $\approx 5$  Å), where the C2-NH was undergoing hydrogen-bonding with the Asp23 side-chain and backbone carbonyl of Val24 (distance  $< 3$  Å). The 4-bromobenzyl isomers (**3k** and **4k**) exhibited nearly opposite binding modes in the dimer model (Figure S4, panel B). The DAQ ring scaffold of **3k** was oriented parallel to the Ser26-Lys28 turn region, where the C2-amine was in contact with the Asp23 side-chain and backbone carbonyl of Val24 (distance = 2.7–3.1 Å). The 4-bromophenyl group was between Asp23 and Ile31 (distance  $\approx 5-6$  Å). In contrast, the corresponding  $N^2$ -isomer **4k** had its DAQ ring scaffold oriented between Ile31/32 and Ala21-Asp23 in a perpendicular fashion, where the C4-amine was hydrogen-bonding with the carbonyl backbone of Ile32 (distance  $\approx 2.7$  Å). The C2-NH was oriented toward Ala30 and was in contact with its carbonyl backbone (distance  $\approx 3$  Å), while the 4-bromophenyl group was stacked, in a parallel orientation, between Asp23 and Gly29 (distance  $\approx 5$  Å). These studies suggest that DAQ ring system serves as a suitable template to design small molecule probes to study A $\beta$  aggregation and inhibition.

In conclusion, we investigated the selective alkylation of the 2,4-diaminoquinazoline (DAQ) template, a privileged scaffold, to generate a library of  $N^2$  and  $N^4$ -substituted DAQ derivatives. These compounds were then screened for antiaggregation properties toward A $\beta$ 40/42 by monitoring their aggregation kinetics, which revealed that halogen-substituted benzyl groups generally exhibited superior anti-A $\beta$  aggregation effect with  $N^4$ -isomers providing better selectivity for A $\beta$ 40, whereas the  $N^2$ -isomers exhibited better inhibition of A $\beta$ 42 aggregation. The  $N^4$ -isomer **3k** with a 4-bromobenzyl substituent was identified as the most potent A $\beta$ 40 aggregation inhibitor ( $\text{IC}_{50} = 80$  nM), whereas the corresponding  $N^2$ -isomer (**4k**) yielded our most potent A $\beta$ 42 aggregation inhibitor ( $\text{IC}_{50} = 1.7$   $\mu\text{M}$ ), which also exhibited dual A $\beta$ 40/42 aggregation inhibition. The outcomes of this study demonstrates the usefulness of quinazoline diamine template to design novel antiamyloid agents. These small molecules serve as valuable pharmacological tools to study and develop potential therapies to treat AD.

## ■ ASSOCIATED CONTENT

### ● Supporting Information

The Supporting Information is available free of charge on the ACS Publications website at DOI: 10.1021/acsmchemlett.6b00039.

Synthetic and biological methods along with characterization and analytical data (PDF)

## ■ AUTHOR INFORMATION

### Corresponding Author

\*Tel: 519-888-4567, ext. 21317. E-mail: [praopera@uwaterloo.ca](mailto:praopera@uwaterloo.ca).

### Author Contributions

P.P.N.R. and T.M. conceived the project and designed the experiments. T.M., A.S., and G.T., performed the experiments. T.M., A.S., and P.P.N.R. analyzed and interpreted the data. T.M. wrote the manuscript. T.M., A.S., G.T., and P.P.N.R. revised the manuscript.

### Notes

The authors declare no competing financial interest.

## ■ ACKNOWLEDGMENTS

The authors would like to thank the Faculty of Science, Office of Research, the School of Pharmacy at the University of Waterloo, Ontario Mental Health Foundation (graduate scholarship for T.M.), NSERC-Discovery (RGPIN: 03830-2014), Canada Foundation for Innovation (CFI-JELF), Ontario Research Fund (ORF), and Early Researcher Award, Ministry of Research and Innovation, Government of Ontario, Canada (PR) for financial support of this research project.

## ■ ABBREVIATIONS

AD, Alzheimer's disease; A $\beta$ , amyloid-beta; DAQ, diaminoquinazoline; DMA, dimethylacetamide; DMSO, dimethyl sulfoxide; NaH, sodium hydride; SAR, structure-activity relationship; DMAP, 4-dimethylaminopyridine; DBU, 1,8-diazabicyclo[7.1.1]undec-7-ene

## ■ REFERENCES

(1) Selkoe, D. J. Cell biology of the amyloid  $\beta$  protein precursor and the mechanism of Alzheimer's disease. *Annu. Rev. Cell Biol.* **1994**, *10*, 373–403.

- (2) LaFerla, F. M.; Green, K. N.; Oddo, S. Intracellular amyloid- $\beta$  in Alzheimer's disease. *Nat. Rev. Neurosci.* **2007**, *8*, 499–509.
- (3) Price, D. L.; Sisodia, S. S.; Gandy, S. E. Amyloid beta amyloidosis in Alzheimer's disease. *Curr. Opin. Neurol.* **1995**, *8*, 268–274.
- (4) Guela, C.; Wu, C.; Saroff, D.; Lorenzo, A.; Yuan, M.; Yanker, B. A. Aging renders the brain vulnerable to amyloid  $\beta$ -protein neurotoxicity. *Nat. Med.* **1998**, *4*, 827–831.
- (5) Hock, C.; Konietzko, U.; Streffer, J. R.; Tracy, J.; Signorell, A.; Muller-Tillmanns, B.; Lemke, U.; Henke, K.; Moritz, E.; Garcia, E.; Wollmer, M. A.; Umbricht, D.; de Quervain, D. J. F.; Hofmann, M.; Maddalena, A.; Papassotiropoulos, A.; Nitsch, R. M. Antibodies against  $\beta$ -amyloid slow cognitive decline in Alzheimer's disease. *Neuron* **2003**, *38*, 547–554.
- (6) Menendez-Gonzalez, M. Biomarkers in neurodegenerative disorders: translating research into clinical practice. *Front. Aging Neurosci.* **2014**, *6*, 1–2.
- (7) Godyn, J.; Jonczyk, J.; Panek, D.; Malawska, B. Therapeutic strategies for Alzheimer's disease in clinical trials. *Pharmacol. Rep.* **2016**, *68*, 127–138.
- (8) Masliah, E.; Rockenstein, E.; Price, D.; Bonhaus, D.; Meier, D.; Moesler, H.; Konrat, R.; Tsigelny, I.; Wrasidlo, W. Small molecules targeting the formation of neurotoxic oligomers for the treatment of AD/PD: a second look. *Neurobiol. Aging* **2014**, *35*, S15.
- (9) Doig, A. J.; Derreumaux, P. Inhibition of protein aggregation and amyloid formation by small molecules. *Curr. Opin. Struct. Biol.* **2015**, *30*, 50–56.
- (10) Ono, K.; Hasegawa, K.; Naiki, H.; Yamanda, M. Curcumin has potent anti-amyloidogenic effects for Alzheimer's  $\beta$ -amyloid fibrils in vitro. *J. Neurosci. Res.* **2004**, *75*, 742–750.
- (11) Hu, S.; Maiti, P.; Ma, Q.; Zuo, X.; Jones, M. R.; Cole, G. M.; Frautschy, S. A. Clinical development of curcumin in neurodegenerative disease. *Expert Rev. Neurother.* **2015**, *15*, 629–637.
- (12) Granzotto, A.; Zatta, P. Resveratrol and Alzheimer's disease: message in a bottle on red wine and cognition. *Front. Aging Neurosci.* **2014**, *6*, 95–102.
- (13) Bastianetto, S.; Menard, C.; Quirion, R. Neuroprotective action of resveratrol. *Biochim. Biophys. Acta, Mol. Basis Dis.* **2015**, *1852*, 1195–1201.
- (14) Jiang, L.; Liu, C.; Leibly, D.; Landau, M.; Zhao, M.; Hughes, M. P.; Eisenberg, D. S. Structure-based discovery of fiber-binding compounds that reduce the cytotoxicity of amyloid beta. *eLife* **2013**, *2*, e00857.
- (15) Rao, P. P. N.; Mohamed, T.; Teckwani, K.; Tin, G. Curcumin binding to beta amyloid: A computational study. *Chem. Biol. Drug Des.* **2015**, *86*, 813–820.
- (16) Hamley, I. W. The Amyloid beta peptide: A chemist's perspective. Role in Alzheimer's and fibrillization. *Chem. Rev.* **2012**, *112*, 5147–5192.
- (17) Soto, C.; Kindy, M. S.; Baumann, M.; Frangione, B. Inhibition of Alzheimer's amyloidosis by peptides that prevent  $\beta$ -sheet conformation. *Biochem. Biophys. Res. Commun.* **1996**, *226*, 672–680.
- (18) Chao, B.; Tong, X.; Tang, W.; Li, D.; He, P.; Garcia, J.; Zeng, L.; Gao, A.; Yang, L.; Li, J.; Nan, F.; Jacobs, M.; Altmeyer, R.; Zuo, J.; Hu, Y. Discovery and optimization of 2,4-diaminoquinazoline derivatives as a new class of potent Dengue virus inhibitors. *J. Med. Chem.* **2012**, *55*, 3135–3143.
- (19) Thurmond, J.; Butchbach, M. E. R.; Palomo, M.; Pease, B.; Rao, M.; Bedell, L.; Keyvan, M.; Pai, G.; Mishra, R.; Haraldsson, M.; Andresson, T.; Bragason, G.; Thosteinsdottir, M.; Bjornsson, J. M.; Coover, D. D.; Burghes, A. H. M.; Gurney, M. E.; Singh, J. Synthesis and biological evaluation of novel 2,4-diaminoquinazoline derivatives as SMN2 promoter activators for the potential treatment of spinal muscular atrophy. *J. Med. Chem.* **2008**, *51*, 449–469.
- (20) Petkova, A. T.; Yau, W. M.; Tycko, R. Experimental constraints on quaternary structure in Alzheimer's  $\beta$ -amyloid fibrils. *Biochemistry* **2006**, *45*, 498–512.